FAST FOURIER TRANSFORM ALGORITHM FOR EXTRACTION OF ATTENUATION, PHASE, AND SCATTERING IMAGES IN PHASE-CONTRAST IMAGING

Ionuț-Cristian CIOBANU[1,2], Nicoleta SAFCA[2,3], Elena ANGHEL[2,4], Cezara RĂȘINAR[1,2], Dan POPESCU[1]

Phase contrast imaging is based on the refraction of the X-ray beam as it passes through the material and shows excellent results for biological tissues. In this paper, we present a new approach for a Python algorithm that can filtrate phase contrast images (attenuation, phase, and scattering) and improve the identification of the interest object. The images used in this work were obtained with a 5.66 m long Talbot-Lau interferometer with a record angular sensitivity of 0.82 μradians, a phase stepping procedure of 16 steps, and a mean energy of 30 keV. The sample used was 0.89 mm diameter fiber from an accredited mammographic phantom. The proposed algorithm extracts the attenuation, phase, and scattering images from the dataset using Fast Fourier Transform. For filtration, we implemented a non-linear filter (median) to eliminate the noise generated by the acquisition system and the projection processing and to improve the contrast. The results were analyzed by calculation of the contrast-to-noise ratio (CNR).

Keywords: Phase-contrast imaging, Fast Fourier Transform, Talbot-Lau Interferometer

1. Introduction

Images obtained by attenuating the X-ray beam, as in conventional X-ray-based imaging methods, have poor contrast, mainly when referring to materials with a low atomic number (*Z*). As the literature shows, phase contrast imaging which is based on the refraction of radiation, provides images with better quality: high spatial resolution and high contrast. This makes materials with a low *Z*, such as soft tissues, more visible. A significant advantage of this technique is that the recorded signal in a single exposure can be separated, thus obtaining three different types of images: attenuation image, phase image/refraction, and scattering/dark field image [1,2].

[1] Faculty of Automatic Control and Computer Science, University POLITEHNICA of Bucharest, Romania
[2] Extreme Light Infrastructure – Nuclear Physics, Magurele, Romania
[3] Engineering and Applications of Lasers and Accelerators Doctoral School (SDIALA), University POLITEHNICA of Bucharest, Bucharest, Romania
[4] Faculty of Chemical Engineering and Biotechnologies, University POLITEHNICA of Bucharest, Romania

Several techniques are used in phase contrast imaging. The most investigated and used in research are [2-5]:

- Propagation-based technique;
- Grating interferometry;
- Crystal interferometry.

The Talbot-Lau interferometry based on gratings is considered the most suitable approach for clinical usage due to its compatibility with standard polychromatic X-ray sources with broad spectrums and relatively large spot sizes. This technique has begun the implementation process toward clinical applications and is very close to achieving this status. An example of its clinical application involves ultrasmall-angle scatter phase contrast imaging of the lungs, which has been successfully tested on patients using a dark-field radiography setup based on gratings. Also, mammography based on grating interferometry is in the research stage but provides good results. Compared to conventional mammography, the images obtained with the grating-based technique are more detailed and the visibility of the malignant structures is improved.[6]

2. Materials and methods

The Talbot-Lau interferometer (Fig. 1) consists of three gratings called *G0*, *G1*, and *G2*, with very small periods of the order of micrometers. Two are absorption gratings (*G0* and *G2*), and one is phase grating (*G1*). Each of them has a specific role [6,7]. The fundamental principle behind this kind of interferometer is the Talbot effect – an element having a periodic structure exhibits a "self-image" effect at a specific distance known as the Talbot distance (d_T). Basically, the *G0* grating is placed in front of the conventional X-ray source to transform the beam into a coherent one. *G1* generates the X-ray interference pattern that can be seen at the Talbot distance (d_T), and *G2*, which is placed in front of the detector, converts the interference pattern into intensity modulations that can be read by the detector. When an object is inserted in the beam path, a small deviation in the trajectory of the incident wave appears by an angle (α) [8]. In Fig 1, a schematic of the experimental Talbot-Lau interferometer setup can be seen.

For the data collection and extraction, the phase-stepping method is used. To obtain the images, one of the gratings is translated into fractional period steps perpendicular to the direction of beam propagation - this is the phase-stepping technique that samples the interference pattern. An image is acquired at each step, and we can extract an almost sinusoidal intensity oscillation curve described using Fourier analysis [9].

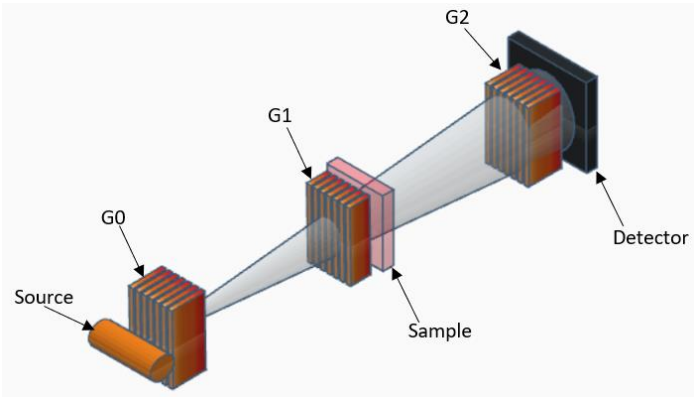

Fig 1. Diagram of the interferometer Talbot-Lau

When the X-ray beam interacts with matter at medical energy ranges, two phenomena occur attenuation and refraction. The photoelectric effect and Compton scattering generally cause attenuation, while refraction is caused by the Rayleigh effect or elastic scattering [10,11].

The attenuation image shows the difference in intensity between measurements without the object (reference/background) and measurements with the object. This image is described by the formula:

$$T = -ln\left(\frac{I_{obj}}{I_{ref}}\right) \quad (1)$$

where T is the transmittance, I_{obj} is the offset of the phase-stepping curve at the moment when the object is inserted, and I_{ref} is the offset of the reference measurement curve [9,10].

The phase image is based on the phase difference that occurs when the X-ray beam passes through the object. This phase difference is related to the refraction angle (α). This type of image can be described as the difference between the phase measured when the analyzed object is inserted and the reference phase [9,10].

The dark-field image is defined as the logarithm in the ratio of visibility of the object (V_{obj}) and reference visibility (V_{ref}). So, the visibility (V) is the ratio between the amplitude of the beam (A) and its intensity (I) [9,10].

The oscillation curves of reference intensity and beam intensity when the object is inserted can be described by Fourier Series [12,13]:

$$I = a_0 + a_1 cos\,(x + \varphi) \quad (2)$$

Fig 2 represents the intensity oscillations obtained from the phase-stepping process of the reference and the object to obtain the attenuation, phase, and scattering images. Thus, with the help of parameters a_0, a_1 și φ, we can extract and calculate the three images we want to obtain. This can be done using the Fast Fourier transform (FFT). Following the calculation of the FFT), parameters a_0, a_1, φ can be extracted according to the equations below:

1. Calculation of coefficients after reference scanning [14]:

$$a_{0r} = |F_0(I_r)| \tag{3}$$

$$a_{1r} = 2 * |F_1(I_r)| \tag{4}$$

$$\varphi_r = \arctan\left(F_1(I_r)\right) \tag{5}$$

2. Calculation of coefficients after scanning the object [14]:

$$a_{0s} = |F_0(I_s)| \tag{6}$$

$$a_{1s} = 2 * |F_1(I_s)| \tag{7}$$

$$\varphi_s = \arctan\left(F_1(I_s)\right) \tag{8}$$

where F_0 and F_1 are the first and second Fourier coefficients [14].

Finally, attenuation, phase, and scattering images can be defined by analogy according to these extracted parameters as [9,10], [15]:

$$T = -ln\left(\frac{a_{0s}}{a_{0r}}\right) \tag{9}$$

$$\Phi = \varphi_s - \varphi_r \tag{10}$$

$$D = \frac{a_{1s}}{a_{0s}} * \frac{a_{0r}}{a_{1r}} \tag{11}$$

where T is the attenuation image, Φ is the phase image, and D is the scattering image.

The paper presents how to acquire the projections of the data set with the Talbot-Lau interferometer and the processing algorithm for extracting attenuation, phase, and scattering images together with filtration. We used the median filter to remove the noise from each type of image and to improve the identification of the interest object.

To obtain the necessary projections for processing, a phase-stepping procedure of 16 steps of 0.3 μm and 40 seconds on each step was performed with the ultrahigh sensitivity Talbot-Lau interferometer developed in the X-ray Imaging Laboratory from Extreme Light Infrastructure – Nuclear Physics (ELI-NP). Subsequently, the dataset processing was carried out using the Python programming language.

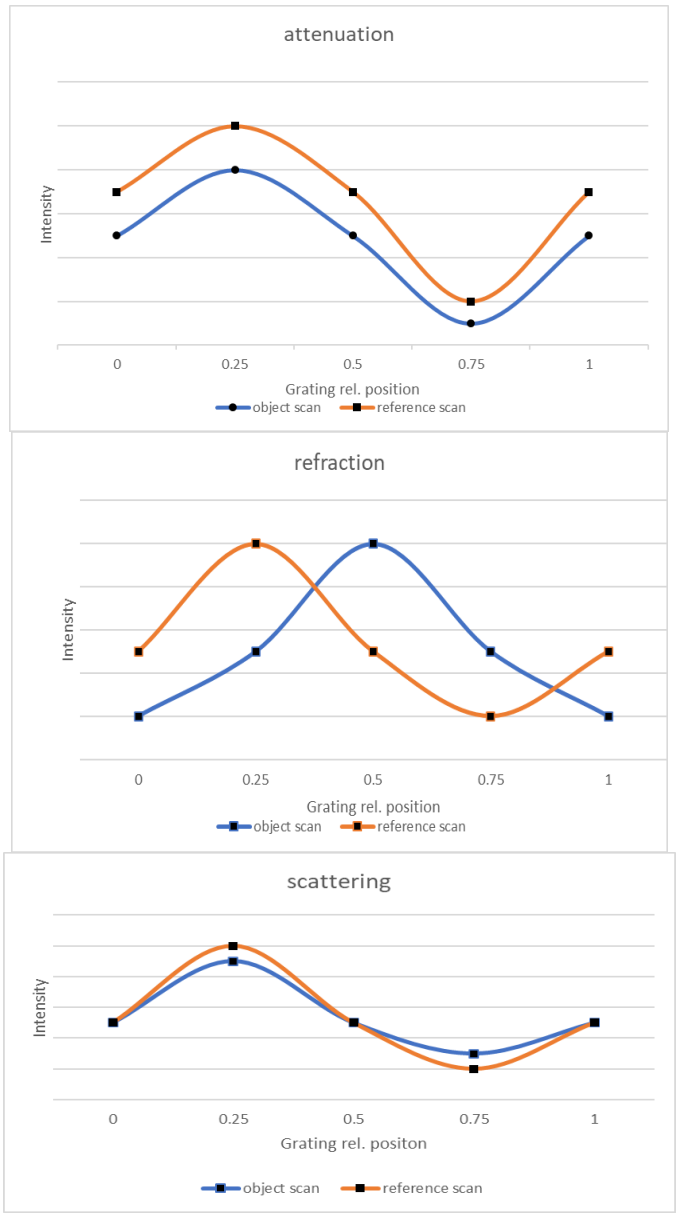

Fig 2. Intensity oscillation curve for each image type

2.1. Obtaining projections

The setup used for obtaining the data set consists of an X-ray tube (the source) with an anode made of tungsten, and the interferometer consists of three microperiodic gratings and an in-house built detector.

The source can generate a variable energy X-ray beam by changing parameters like voltage and current. X-rays can be generated by applying a voltage in the 20-160 kV range and a current in the 1-20 mA range. A Talbot-Lau interferometer consisting of the three gratings (*G0*, *G1*, *G2*) is used (Fig.3). The source (X-ray tube) is a conventional one, so *G0* is used to make the beam coherent after passing through this grating. *G1* produces the interference pattern, and *G2* converts this interference pattern into intensity modulations.

Table 1 shows the materials from which the gratings are made, their period, and the height of the deposited material.

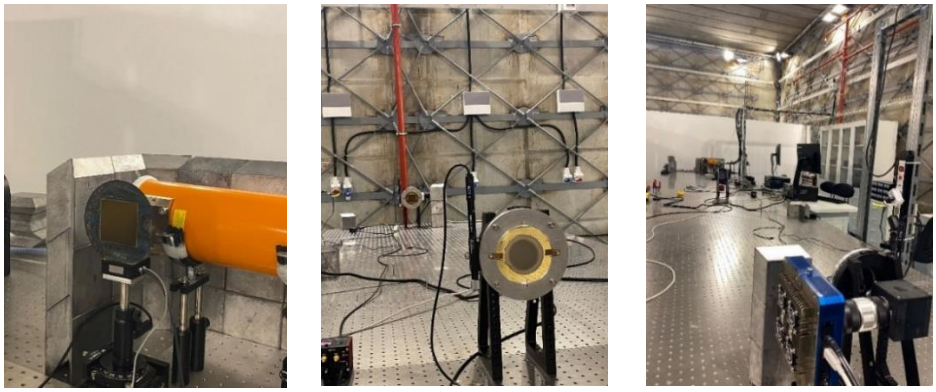

a) b) c)

Fig 3. Experimental assembly: a) grating *G0*, b) rating *G1* and *G2* (b), and c) all experimental set-up

Table 1

Parameters of gratings

Grating	Material	Period (μm)	Thickness (μm)
G0	Gold	2.4	55
G1	Nichel	2.4	8.6
G2	Gold	2.4	57

Both *G0* and *G2* are absorption gratings. They were made of a material with a high atomic number, gold, and were deposited in a layer larger than the nickel deposition of the phase grating. The thickness of the gratings is limited by fabrication. These are the smaller gratings available in the markets. Another element inside the experimental assembly is the detector. In this experiment, a detector composed of a scintillator, lens, and a visible CCD camera were used.

To obtain projections with the phase-stepping technique, the G0 grating was placed on a piezo stage that can be moved in micrometer steps. The operating parameters of the source were 30 kV and 15 mA, and every projection was obtained with an exposure of 40 s. Also, the phase-stepping procedure was applied over two periods with 16 steps of 0.3 μm.

The sample used is a nylon fiber inside an accredited medical phantom Gammex 156 [16]. This phantom (Fig. 4a) imitates 4.2 cm of compact breast composed of 50% fibrous tissue and 50% adipose tissue. Gammex 156 contains 16 objects that reproduce various tissues or malignant tumors of the breast [16].

The chosen fiber to analyze in this study was a 0.89 mm diameter fiber. This is indexed in Fig 4b under number 3. The fiber is made of nylon and is embedded in wax. The purple circle represents the background (reference) we used.

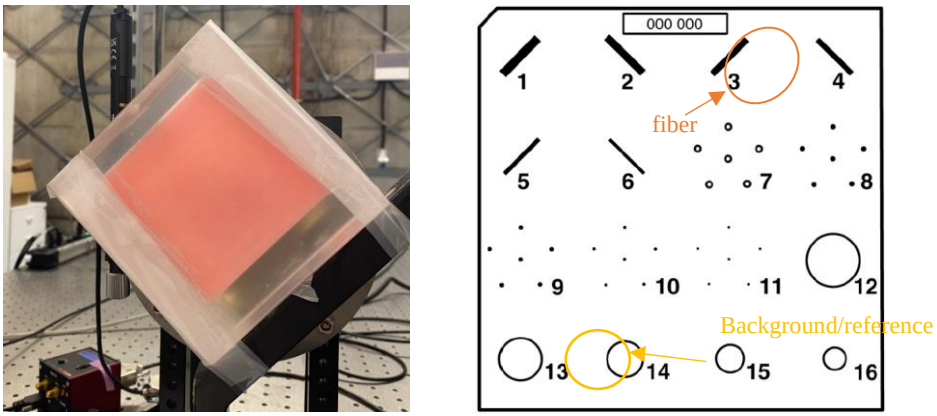

a) b)

Fig. 4. a) Mammography phantom used. b) distribution of its structures

2.2 Algorithm

Following the phase-stepping procedure, the proposed algorithm analyzes and processes images to extract information about attenuation, phase, and scattering. Thus, three types of images can be obtained that highlight different tissue properties.

The algorithm was implemented in the Python programming language. This programming language is an accessible language to learn and use. Because of this, Python is used in many areas, such as web development, business applications, and scientific computing. This language has many standard libraries with many functionalities and predefined modules. Python is a free and open-source language with the freedom to redistribute and contribute to developing different libraries [17]. Fig. 5 shows schematically all the steps of the algorithm. The parameter extraction is done using formulas (3)-(8), and the images are obtained according to formulas (9)-(11).

Two functions have been implemented to apply a median filter in the filtration step. The first function receives as parameters the analyzed images and the size of the pixel neighborhood (k). Pixel neighborhood represents a window of

dimensions (2*k+1)x(2*k+1). This function checks that the neighborhood of the pixels is fully included in the image and calls the second function, which takes the neighborhood of each pixel in a flattened vector and takes the median value. The resulting median value is then assigned to the corresponding pixel in the final image. This filter is applied to remove the noise due to processing the three images. This is generated by dividing the extracted values by zero.

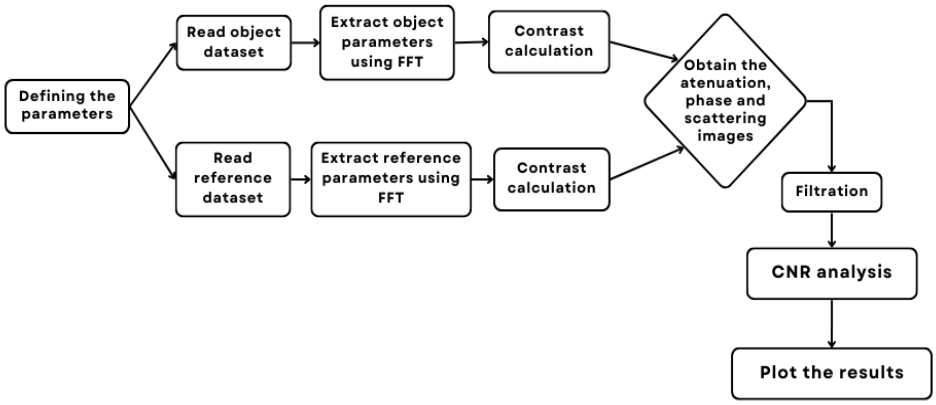

Fig. 5. Schematic representation of the algorithm.

3. Experimental results and discussions

To obtain the attenuation, phase, and scattering images, 32 projections were used. Of these, 16 projections contain the object of interest, and the others contain the reference/background. These were obtained by phase-stepping technique with the Talbot-Lau interferometer in the X-ray Imaging Laboratory at ELI-NP at exposures of 40 s for each phase-stepping step and a 30 keV mean energy.

These projections were read with the Python code explained above, obtaining the results to be represented below, step by step. Figure 6 represents the raw image with the object of interest and the other the raw image of the reference (background). Fig. 6a shows a projection of 0.89 mm nylon fiber, and Fig. 6b is a projection of the reference. Reference images consist of exposures of areas that do not contain fiber, tumors, or calcifications. In the case of the breast phantom analyzed in this paper, the reference area is a portion that contains only wax.

The contrast of these images was calculated using the average of a 5x5 size fixed window by the contrast formula [18]:

$$C = \frac{V_{max} - V_{min}}{V_{max} + V_{min}} \tag{12}$$

where C is the value of contrast, V_{min} is the smallest of the calculated averages, and V_{max} is the highest of the calculated averages. For this particular configuration, a

contrast of 10.6% was obtained for the nylon fiber images, while for the background images, a contrast of 11.3% was obtained.

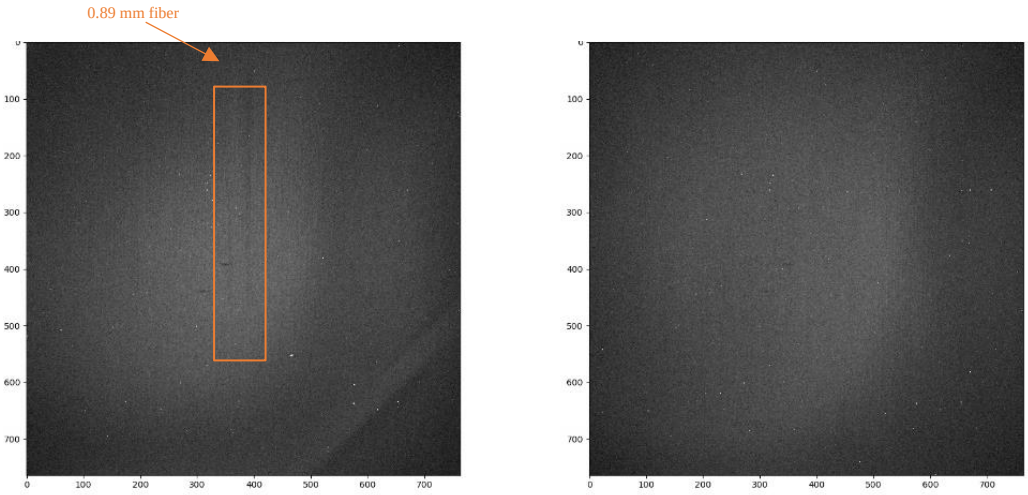

a) Image with the object b) Image without the object (background/reference)

Fig 6. An image from the dataset with the object (a) and an image from the dataset without the object (b),

The parameters φ_s, $a_{0s,}$ and a_{1s} are the phase, attenuation, and scattering parameters for the nylon fiber images, while φ_r, $a_{0r,}$ and a_{1r} are the phase, attenuation, and scattering parameters for reference. These parameters were extracted using equations (3)-(8), and they can be seen in Fig 7. φ_s, $a_{0s,}$ $a_{1s,}$ φ_r, $a_{0r,}$ and a_{1r} are used to obtain attenuation, phase, and scattering images.

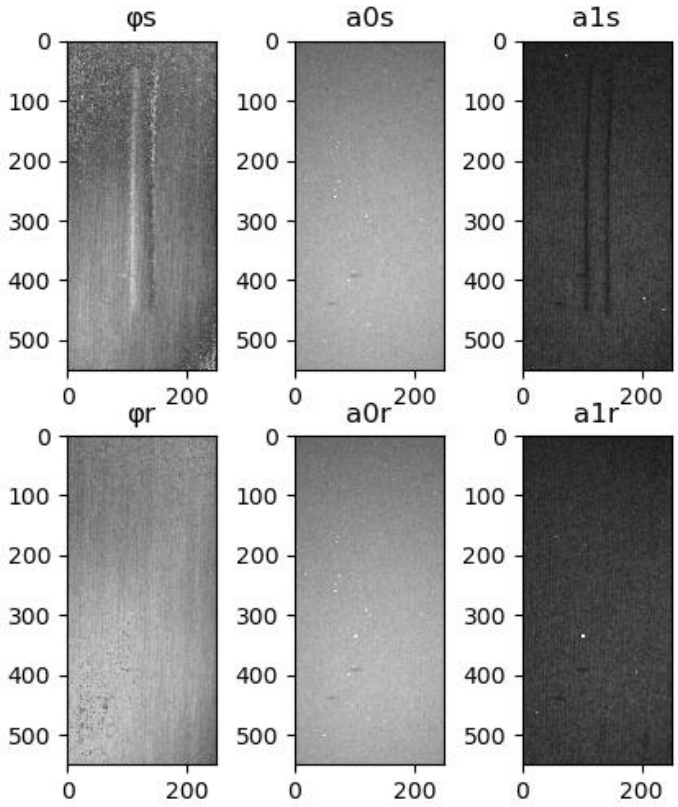

Fig 7. Parameters extracted with FFT

Equations (9), (10), and (11) were used to obtain the images of attenuation, phase, and scattering. The noise in the images is relatively high. This effect can be seen in Fig 8. It can be due to both hardware components and how these three images were processed. An example might be the appearance of white pixels due to divisions by the value of zero. At the same time, in the case of phase images, the appearance of noise may be due to the incomplete elimination of the interference pattern, so we can still see the maximum from the interference pattern initially generated.

The attenuation image with an exposure of 40 s does not provide much detail, and the fiber is almost invisible. The phase image provides a pseudo-3D visualization of the analyzed object, and the edges of the fiber are well-evident. The dark field image can provide information about the outline of the analyzed objects.

Also, the images obtained are affected by noise. The attenuation and scattering images have noise caused by the extraction process. The noise from the phase image was generated by the hardware system. This type of artifact appears because of the incomplete elimination of the interference pattern and scattering effects.

To improve the quality of the images and to eliminate noise, a median filter was applied, and the result can be seen in Fig 9. For the attenuation image, it was enough to choose a neighborhood 3x3 to eliminate noise, while for phase and scatter images, a neighborhood 5x5 was used.

As it can be seen, the noise is reduced, but the edges of the fiber start to blur. So, when this kind of filtering is applied, we should pay attention to the value of the size pixel neighborhood (*k*). For a big value of *k*, the images can be blurred and we can lose some details.

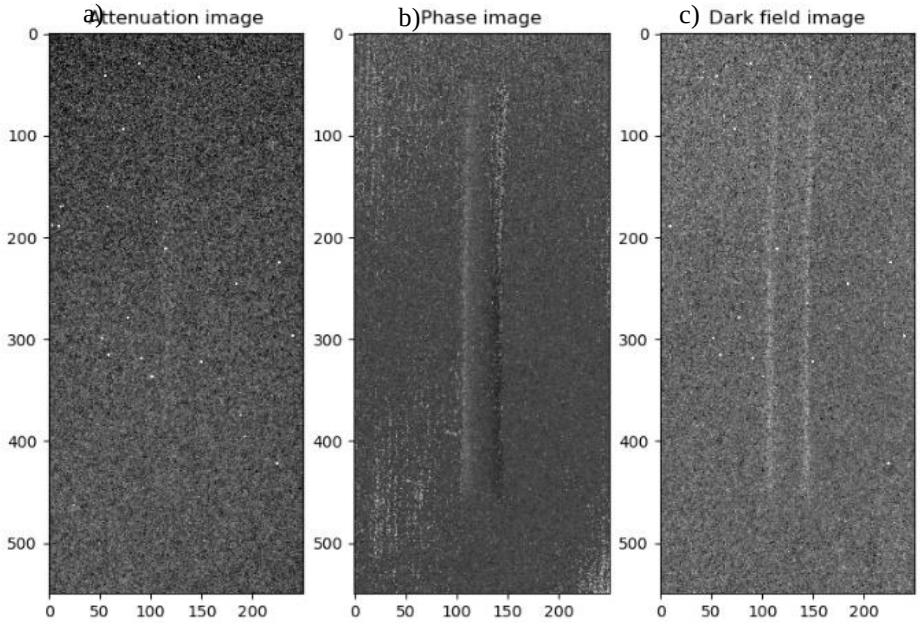

Fig 8. Attenuation (a), phase (b), and scattering/dark field (c) images.

This method can provide three different images with a single exposure and has the potential to render different information about the analyzed objects. More than that, according to [6], the absorbed dose for exposure of 512 s with this technique is 2.73 mGy. Using the same method, for an exposure of 640 s (16 steps of 40 s), the dose in the case presented in this paper is 3.41 mGy. The dose is comparable with the conventional technique (3-5 mGy) [19].

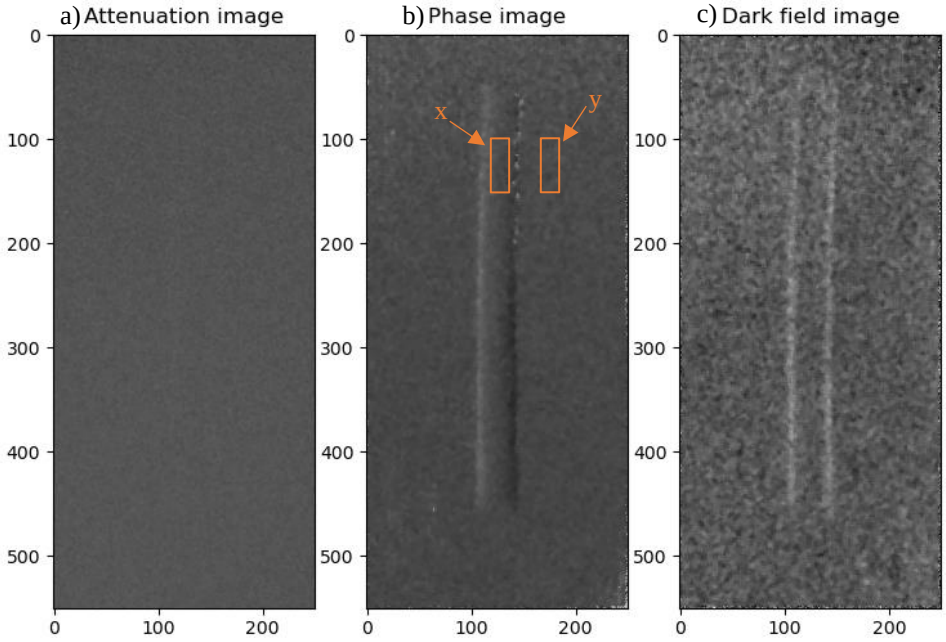

Fig. 9. Attenuation (a), phase (b), and scattering/dark field (c) images processed with a median filter

The contrast-to-noise ratio (CNR) was also calculated for the three extracted images using the same method as in [6]. So, the CNR is the difference between the mean pixel values in the signal and the mean pixel values in the background, divided by the standard deviation of the background [6],[20]:

$$CNR = \frac{mean(x) - mean(y)}{std(y)} \tag{13}$$

where *x* is a part of fiber and *y* is a part of the background. We calculated the mean of pixel values and the standard deviation for the orange highlighted parts from Fig. 9. Also, we mention that x and y were positioned in the same places for every type of image. We obtained the CNR for the attenuation, phase, and scattering images, and the results are displayed in Table 2.

Table 2

CNR for attenuation, phase, and scattering images

	Attenuation image	Phase image	Scattering image
CNR before filtration	0.13	1.1	0.81
CNR after filtration	0.26	5.66	1.09

As can be seen, the value of CNR is very small for the attenuation image. This is to be expected because the fiber is almost invisible in this image. The biggest value of CNR is for the phase image, which provides the most fiber details. Also, the CNR increases after filtration by 80% in the phase image.

We used this algorithm on other data sets consisting of 160 projections (80 projections with the object and 80 projections with the background), so we obtained 15 more images (5 attenuation images, 5 phase images, and 5 scattering images). Each dataset was acquired at different exposure times and different energies. We made the CNR calculation and we observed that every phase and scattering images obtained has an increase of CNR after filtration. All the phase images obtained from this data sets have an increase of CNR after filtration of more than 78%. The biggest increase in CNR is about 90%.

4. Conclusions

We used a 5.66 m long grating-based interferometer with a record angular sensitivity of 0.82 μradians and a fringe contrast of 11% to obtain the datasets by applying a phase-stepping procedure of 16 steps of 0.3μm and an exposure time of 40 seconds per each step at a mean energy of 30 keV. As the results and literature show, this type of radiography has the potential to become an additional tool for X-ray imaging applications.

The algorithm implemented has the purpose of extracting the three types of images (attenuation, phase, and scattering images) by analyzing the phase shift from the datasets and aims to increase the contrast of the images to improve the identification of the interest object. We implemented a median filter and analyzed the performance of our system using the CNR.

Images obtained after extraction are affected by artifacts resulting from processing, but with the application of a median filter, noise is eliminated, and image quality increases. The biggest improvement in visibility is in the phase image. The improvement after filtration is in the range of 78%-90%. The algorithm we implemented provides a simple way to eliminate the noise, increase the quality of the images, and improve the identification of the fiber by application of a basic non-linear filtration.

R E F E R E N C E S

[1] *S. Tao, C. He, X. Hao, C. Kuang and X. Liu*, Principles of Different X-ray Phase-Contrast Imaging: A Review, Appl. Sci., 2021.

[2] *U. Bonse și M. Hart*, An X-ray interferometer, Appl. Phys. Lett, 1956.

[3] *T. Weitkamp, A. Diaz, C. David, F. Pfeiffer, M. Stampanoni, P. Cloetens și E. Ziegler,* X-ray phase imaging with a grating interferometer, Opt. Express, 2005.

[4] *A. Snigirev, I. Snigireva, V. Kohn, S. Kuznetsov și I. A Schelokov*, On the possibilities of x-ray phase contrast microimaging by coherent high-energy synchrotron radiation, Rev. Sci. Instrum., 1995.

[5] *N. Safca, P. Ghenunghe, C. A. Ur și D. Stutman*, PERSPECTIVE ON USING TALBOT-LAU X-RAY PHASE, UPB Sci. Bull., 2021.

[6] *N. Safca, D. Stutman, E. Anghel, F. Negoita și C. A. Ur*, Experimental demonstration of ultrahigh sensitivity Talbot-Lau interferometer for low dose mammography, Physics in Medicine & Biology, 2022.

[7] *D. Stutman, T. J. Beck, J. A. Carrino și C. O. Bingham*, Talbot phase-contrast X-ray imaging for the small joints of the hand, Physics in Medicine and Biology, 2011.

[8] *L. Birncacher*, High-sensitivity grating-based phase-contrast computed tomography with incoherent sources, Master Thesis, Technische Universitat Munchen, 2018.

[9] *A. Sarapata*, Quantitative X-ray imaging with high-energy grating interferometry at conventional sources, PhD. Thesis, Technische Universitat Munchen, 2015.

[10] *M. Seifert*, Optimisation of image reconstruction for Talbot-Lau x-ray phase-contrast imaging with regard to mechanical robustness, Master Thesis, Friedrich-Alexander-Universitat Erlangen-Nurnberg, 2016.

[11] *F. M. Epple*, Contributions to X-ray Phase-Contrast Imaging with an Energy-Sensitive Photon-Counting Detector, PhD. Thesis, Technische Universitat Munchen, 2015.

[12] *P. Picart*, Interferometry and fringe pattern demodulation, 2007.

[13] *F. D. Marco, M. Marschner, L. Birnabacher, P. Noel, J. Herzen and F. Pfeiffer*, Analysis and correction of bias induced by phase stepping jitter in grating-based X-ray phase-contrast imaging Optics Express , 2018.

[14] *R. Kaufmann, M. Plamondon, J. Hofmann și A. Neels*, Comparison of different phase retrieval algorithms, SPIE, 2017.

[15] *C. Wu, L. Zhang, Z. Chen, Y. Xing, X. Li și X. Zhu,* The trigonometric orthogonality of phase-stepping curves in grating-based x-ray phase-contrast imaging: Integral property and its implications for noise optimization, 2020.

[16] „doza.ru," [Interactiv]. Available: https://www.doza.ru/docs/med/fma.pdf. [Accesat 15 06 2023].

[17] „python.org," [Interactiv]. Available: https://www.python.org/about/apps/. [Accesat 18 06 2023].

[18] *Y. Y. Kachurin, A. V. Kryukov, O. A. Kananykhin și A. V. Fedorinov*, Calculation of contrast for computer simulated resolution chart image, J. Phys.: Conf. Ser, 2021.

[19] „www.iaea.org," [Interactiv]. Available: www.iaea.org. [Accesat 29 06 2023].

[20] *E. Eggl, S. Grandl, A. Sztrókay-Gaul et. al.*, Dose-compatible grating-based phase-contrast mammography on mastectomy specimens using a compact synchrotron source, Sci. Rep., 2018.